Universal Scaling of the Velocity Field in Crack Front Propagation

Clément Le Priol,[1,*] Julien Chopin,[2] Pierre Le Doussal,[1] Laurent Ponson,[3] and Alberto Rosso[4]
[1]CNRS–Laboratoire de Physique de l'Ecole Normale Supérieure, 24 rue Lhomond, 75231 Paris Cedex, France
[2]Instituto de Física, Universidade Federal da Bahia, Salvador-BA, 40170-115, Brazil
[3]Institut Jean le Rond d'Alembert, Sorbonne Université, 75252 Paris Cedex 05, France
[4]LPTMS, CNRS, Université Paris-Sud, Université Paris-Saclay, 91405 Orsay, France

(Received 20 September 2019; revised manuscript received 11 December 2019; accepted 15 January 2020; published 11 February 2020)

The propagation of a crack front in disordered materials is jerky and characterized by bursts of activity, called avalanches. These phenomena are the manifestation of an out-of-equilibrium phase transition originated by the disorder. As a result avalanches display universal scalings which are, however, difficult to characterize in experiments at a finite drive. Here, we show that the correlation functions of the velocity field along the front allow us to extract the critical exponents of the transition and to identify the universality class of the system. We employ these correlations to characterize the universal behavior of the transition in simulations and in an experiment of crack propagation. This analysis is robust, efficient, and can be extended to all systems displaying avalanche dynamics.

DOI: 10.1103/PhysRevLett.124.065501

The presence of disorder is often at the origin of physical behaviors that are not observed in pure systems. In particular, under a slow drive, a disordered system does not respond smoothly but is characterized by quick and large rearrangements called *avalanches* followed by long quiescent periods. The earthquakes in tectonic dynamics [1–3], the plastic rearrangements in amorphous materials [4,5] or the Barkhausen noise in soft magnets [6–8] are examples of such avalanches. If the drive is very slow, avalanches are triggered one by one: the system is driven to a first instability and then evolves freely until it stops. In this *quasistatic limit* one can measure the size and the duration of each avalanche. Their statistics are scale free on many decades, revealing a critical behavior independent of many microscopic details.

This behavior is well established for earthquakes and Barkhausen noise where events are well separated in time. However, in most experimental systems, the driving velocity is finite, so that a subsequent avalanche is often triggered before the previous one stops. One of the standard propositions to define avalanches is to threshold the *global* velocity signal. However, this kind of analysis raises important issues: If the threshold is too large, a single avalanche may be interpreted as a series of seemingly distinct events, while if it is too small subsequent avalanches can be merged into a single event [9–12]. Hence, disentangling avalanches becomes nearly impossible and accurately measuring critical exponents is then particularly challenging. An alternative method to define avalanches is to threshold the local velocity signal in order to establish the state (quiescent or active) of each point in the system [13]. The issue is then to decide whether two active regions separated in space and/or time do belong to the same avalanche or not. The latter problem is particularly severe when studying the propagation of cracks [14–17] and wetting fronts [18–20] in disordered materials. In these systems, the interactions are proven to be long ranged [21,22] and quasistatic avalanches are spatially disconnected objects [23]. Hence, reconstructing avalanches from the resulting map of activity clusters remains very difficult, as for large systems there are active points at any time.

In this Letter, we develop an alternative strategy. We show that the study of the space and time correlations of the local velocity field, a quantity which is experimentally accessible, allows us to capture the universal features of the dynamics without any arbitrariness or any tunable parameter, even at a finite driving speed. We propose and characterize the scaling forms of these functions and show how they relate with the critical exponents of the avalanche dynamics and with the range of the interactions in the system. Our predictions are tested on numerical simulations and experimental data of crack propagation, but are expected to hold for all systems displaying avalanche dynamics but driven at finite velocity.

In Fig. 1 we show a sketch of the crack front where $u(x,t)$ is the front position at point x and time t. Its equation of motion in adimensional units writes [see Eq. (11) of the Supplemental Material [24] and also [25–28]]

$$\frac{v(x,t)}{\mu} = f + \eta[x, u(x,t)] + \frac{1}{\pi}\int \frac{u(x',t) - u(x,t)}{|x'-x|^{1+\alpha}}\,dx', \quad (1)$$

with $v(x,t) = \partial_t u(x,t)$. The mobility μ has the dimension of a velocity. In an ideal elastic material it coincides

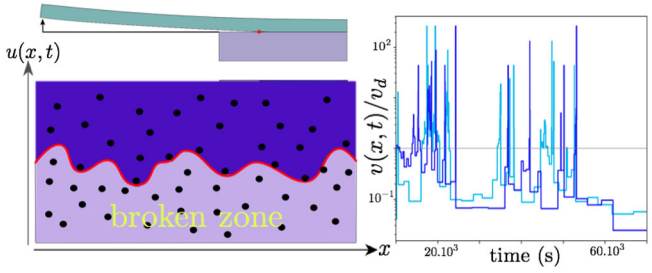

FIG. 1. Left: Sketch of the experimental setup of planar crack propagation. Profile view (top left): a Plexiglas plate is detached from a thick silicone substrate at fixed velocity. Top view (bottom left): the crack front (red line) separates the broken region from the unbroken one. Defects are dots of diameter $d_0 = 100\ \mu$m. Right: Local velocity of two points which are $3d_0$ apart along the front. The gray line corresponds to the average speed v_d. Each signal is intermittent and the two signals display clear correlations.

with the Rayleigh velocity c_R but it is in general, much smaller [24]. The first term is the adimensional force f which drives the crack propagation, $\eta(x,u)$ is the normalized toughness fluctuations and the last term accounts for the elasticity along the interface. In general, this interaction is long range with $0 < \alpha \leq 2$ ($\alpha = 2$ corresponds to short-range elasticity). In particular, for the crack [29] and the wetting fronts [22] it was shown that $\alpha = 1$.

The competition between elasticity and disorder in (1) is at the origin of a second order dynamical phase transition called depinning [30,31]. The force f is the control parameter and the velocity v is the order parameter which vanishes at a critical force f_c. In analogy with equilibrium phase transitions, two independent exponents can be defined: the exponent β associated with the order parameter $v \sim (f - f_c)^\beta$ and the roughness exponent ζ associated with the fluctuations of the front position $\langle [u(x,t) - u(0,t)]^2 \rangle \sim x^{2\zeta}$; the brackets $\langle \ldots \rangle$ denote the average over different realizations of the disorder.

Below f_c the velocity is zero, but a local perturbation can induce an extended reorganization of the front, the *avalanche*, up to a scale $\xi \sim |f - f_c|^{-\nu}$, the divergent correlation length of the transition. Symmetries and dimensional analysis allow us to link all the exponents of the avalanche statistics (size, duration,…) to β and ζ. In particular, the statistical tilt symmetry ensures the scaling relation $\nu = 1/(\alpha - \zeta)$.

In the moving phase it is customary to work with a fixed driving velocity v_d instead of a fixed force f. In practice, this is achieved by replacing f with a parabolic potential of curvature m^2 moving at velocity v_d: $f \to m^2[v_d t - u(x,t)]$ [24]. When v_d is small, the local velocity field $v(x,t)$ along the front displays two features which are a clear manifestation of the presence of avalanches: (i) it is very intermittent in time, i.e., it is either large of order $v^{\max} \gg v_d$ or almost zero and (ii) it displays strong correlations in space (see Fig. 1 right). Instead of trying to identify avalanches we focus on this quantity and its correlation functions

$$C_v(x) \coloneqq \langle v(0,t)v(x,t)\rangle - v_d^2 = v_d^2 \mathcal{F}\left(\frac{x}{\xi_v}\right), \quad (2)$$

$$G_v(\tau) \coloneqq \langle v(x,t)v(x,t+\tau)\rangle - v_d^2 = v_d^2 \mathcal{G}\left(\frac{\tau}{t^*}\right). \quad (3)$$

The proposed scaling forms rely on the existence of two scales: $\xi_v \sim v_d^{-\nu/\beta}$ and $t^* \sim v_d^{-\nu z/\beta}$. The first one is the correlation length at finite velocity and arises naturally from the combination of the scalings of the velocity $v \sim (f - f_c)^\beta$ and of the correlation length $\xi \sim (f - f_c)^{-\nu}$. The time scale t^* is linked to ξ_v through the dynamical exponent z [32]: $t^* \sim \xi_v^z$. Note that these assumptions are reasonable provided that m^2 is small enough, otherwise the parabolic potential confines the interface at length scales $\sim m^{-2/\alpha}$.

Asymptotic forms.—We derive the asymptotic forms of $\mathcal{F}(y)$ and $\mathcal{G}(y)$ via a scaling analysis based on the existence of a unique correlation length (and a unique correlation time) when v_d is small. Below this length (and time), one expects to find the critical behavior while above it, the $f \to \infty$ behavior (equivalent to $v_d \to \infty$) should be recovered. For a slow drive $v_d \to 0$, the local velocity is intermittent: it takes values of order $v^{\max}$ (independent of v_d) with probability $\propto v_d$ and is almost zero otherwise. The main contribution to $C_v(x)$ comes from the realizations for which both $v(0,t)$ and $v(x,t)$ are of order $v^{\max}$. In the critical regime, one expects from dimensional analysis that if $v(0,t)$ is of order $v^{\max}$, then $v(x,t)$ is also of order $v^{\max}$ with a probability that decays as $x^{-\beta/\nu}$ [33]. This gives $C_v(x) \sim v_d x^{-\beta/\nu} \sim v_d^2 (x/\xi_v)^{-\beta/\nu}$. For temporal correlations, a similar reasoning yields $G_v(\tau) \sim v_d \tau^{-\beta/(\nu z)} \sim v_d^2 (\tau/t^*)^{-\beta/(\nu z)}$.

Concerning the large scale behavior, it is convenient to rewrite Eq. (1) in the comoving frame: $u(x,t) \to v_d t + u(x,t)$ and neglect the parabolic drive. The disorder becomes $\eta[x, v_d t + u(x,t)]$. From dimensional analysis one sees that at large scales, when $x > \xi_v$ or $t > t^*$, u is subdominant compared to $v_d t$ (see Appendix B [24]). Then the behavior of Eq. (1) is captured by a linear Langevin equation that we solve in Appendix B [24]. By plugging the solution into the correlation function we obtain

$$C_v(x \gg \xi_v) \sim \begin{cases} 1/x^{1+\alpha} & \text{for } \alpha < 2, \\ e^{-x/\xi_v} & \text{for short range,} \end{cases} \quad (4)$$

$$G_v(\tau \gg t^*) \sim -1/\tau^{1+\frac{1}{\alpha}} \quad \text{for } \alpha \leq 2. \quad (5)$$

Note that at a large distance, the decay of the spatial correlation function provides exactly the range $1 + \alpha$ of the elastic interactions. Interestingly, the longtime behavior of $G_v(\tau)$ displays anticorrelations with an α dependent

power law decay. We note a qualitative similarity with the anticorrelation between the sizes of dynamical avalanches, predicted and numerically measured in [34]. Collecting all of this information, we can write the full scaling forms (here for $\alpha = 1$, i.e., for crack and wetting fronts):

$$\mathcal{F}(y) \sim \begin{cases} y^{-\beta/\nu} & \text{if } y \ll 1, \\ y^{-2} & \text{if } y \gg 1, \end{cases} \tag{6}$$

$$\mathcal{G}(y) \sim \begin{cases} y^{-\beta/\nu z} & \text{if } y \ll 1, \\ -y^{-2} & \text{if } y \gg 1. \end{cases} \tag{7}$$

Simulation and experiment.—We implemented a cellular automaton version of the variant of Eq. (1) with f replaced by $m^2[v_d t - u(x,t)]$ and $\alpha = 1$. The three variables u, x, and t are integer. In particular, we assume periodic boundary conditions along x which take values ranging from 0 to $L-1$. The local velocity is defined as

$$v(x,t) = \theta\{F(x,t) + \eta[x, u(x,t)]\},$$
$$F(x,t) = m^2[v_d t - u(x,t)] + \sum_{x'} \frac{u(x',t) - u(x,t)}{|x' - x|^2}, \tag{8}$$

θ being the Heaviside function. Here, the quenched disorder pinning force η should be negative and uncorrelated. In practice, we take identical and independent variables whose distribution is the negative part of the normal law. At each time step all the points feeling a positive total force jump one step forward while the other points—which feel a negative force—stay pinned. Then the time is incremented, $t \to t+1$, and the forces are recomputed: new pinning forces are drawn for the jumping points, the elastic force is updated by using a fast fourier transform algorithm and the driving force is incremented by $m^2 v_d$. For the numerical implementation, we started from a flat configuration, turned on the dynamics, and waited until reaching the steady state before computing the two correlation functions.

The experimental data presented here correspond to planar crack propagation. A 5 mm thick Plexiglas plate is detached from a thick silicone substrate using the beam cantilever geometry depicted in Fig. 1 [35]. To introduce disorder, we print obstacles of diameter $d_0 = 100$ μm with a density of 20% on a commercial transparency that is then bonded to the Plexiglas plate. Crack front pinning results from the strong adhesion of the ink dots to the substrate. Images of 1800×1800 pixels are taken normal to the mean fracture plane every second. As the system is fully transparent, the crack front appears as the interface between the clear and the dark region observed on the image. The pixel size is 35 μm, so the observed front length is 63 mm.

We tested two different velocity regimes: $v_1 = 132 \pm 3$ nm s^{-1} and $v_2 = 31 \pm 1$ nm s^{-1}. The local crack speed is computed using the methodology proposed in Refs. [13,36] based on the waiting time matrix: the number of frames during which the front stays inside each pixel provides the waiting time in this pixel, from which the local speed is inferred.

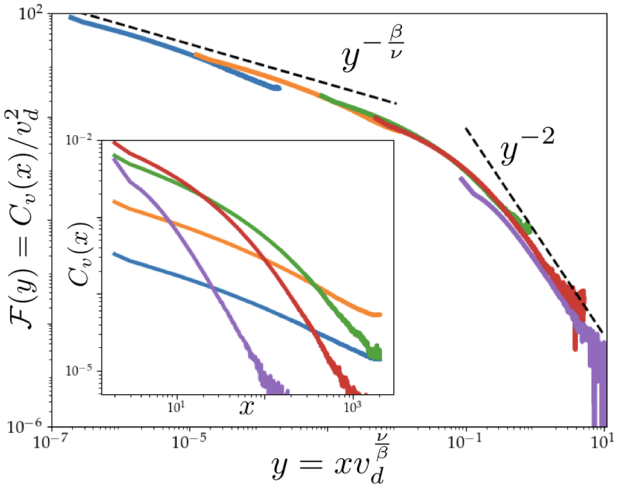

FIG. 2. Spatial correlations in the cellular automaton for driving velocities $v_d = 0.002$ (blue), 0.01 (yellow), 0.05 (green), 0.1 (red), and 0.3 (purple). *Main panel:* A perfect collapse is observed using the scaling form (2). The asymptotic behaviors (6) are verified. In particular, going at large distances the decay y^{-2} of the elastic interaction is recovered while at small distances the critical behavior $\beta/\nu \simeq 0.385$ is captured. From the crossover the length ξ_v is estimated to be $\xi_v \simeq 0.07 v_d^{-\nu/\beta}$. *Inset:* Non-rescaled correlation function $C_v(x)$. System size: $L = 4096$, mass: $m^2 = 10^{-3}$.

Both experiments and the cellular automaton are expected to belong to the universality class of a one dimensional interface with $\alpha = 1$. The depinning exponents of this class have been computed numerically: $\zeta = 0.388 \pm 0.002$ [37], $\nu = 1/(1-\zeta) = 1.634 \pm 0.005$, $\beta = 0.625 \pm 0.005$, $z = 0.770 \pm 0.005$ [38] in agreement with renormalization group calculations [39]. The spatial correlations of the local velocity are shown on Figs. 2 and 3. The results of the simulation perfectly collapse on the scaling form (2) showing that a unique correlation length ξ_v controls the dynamics. The asymptotic form proposed in (6) is verified, in particular the decay in $1/x^2$ is the fingerprint of the long-range nature of the elasticity.

Our experiment confirms the large distance decay as $1/x^2$. This proves that the elastic kernel of the crack front is long range in this experiment [35]. For both velocities the large scale behavior breaks down for distances of 2–3 pixels. This is consistent with our estimation $\xi_v \simeq 2d_0$ at the end of Appendix A [24]. At variance with the simulation, varying the crack speed v_d does not affect the scale ξ_v. This rather counterintuitive behavior results from the velocity dependence of the material toughness [40]. This induces that the characteristic mobility μ involved in Eq. (1) scales with the mean crack speed v_d so that the

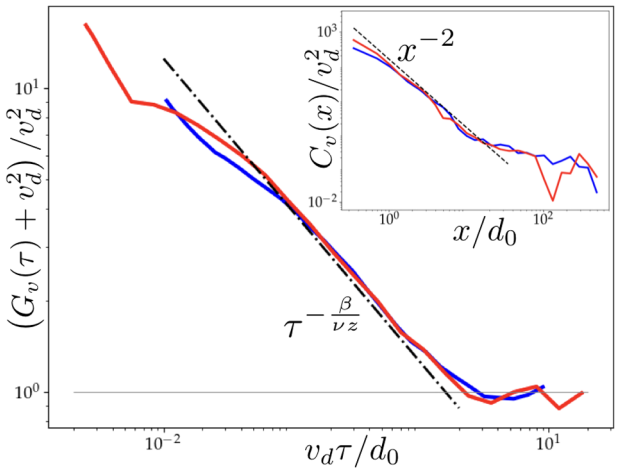

FIG. 3. *Inset*: Spatial correlations in the experiment for driving velocities $v_1 = 132$ nm/s (blue) and $v_2 = 31$ nm/s (red). The large distance decay x^{-2} of the elastic interactions is observed. No rescaling of the x axis was performed. *Main panel*: Temporal correlations for the same velocities. The asymptotic predictions of (7) are verified: anticorrelations are observed at large time and the depinning power law decay is recovered at short time. The time axis was rescaled by v_d.

distance v_d/μ to the critical point remains constant [41] (see [35] and the last section of Appendix A [24]).

We now turn to the temporal correlation function. The results are shown on Figs. 3 and 4 where we plot the correlation function $G_v(\tau) + v_d^2$ and normalize it by

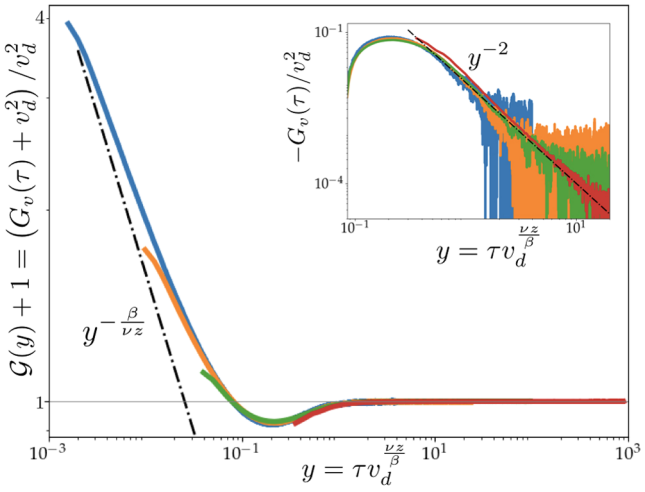

FIG. 4. Temporal correlations in the cellular automaton for driving velocities $v_d = 0.02$ (blue), 0.05 (yellow), 0.1 (green), and 0.3 (red). *Main panel*: The scaling form (3) and the asymptotic behaviors (7) are verified. In particular, at large time we observe anticorrelations while at small time the depinning behavior $y^{-\beta/(\nu z)}$ is recovered ($\beta/(\nu z) \simeq 0.500$). *Inset*: Enlargement on the anticorrelation. For $\alpha = 1$ the expected decay is $1/y^2$. System size: L and m range from $L = 2048$, $m^2 = 10^{-3}$ ($v_d = 0.3$) to $L = 32768$, $m^2 = 10^{-4}$ ($v_d = 0.02$).

dividing by v_d^2. The parts of the curves below 1 correspond to anticorrelation. Again, numerical simulations show a perfect collapse on the scaling form (3) with a unique t^* and the asymptotic form of Eq. (7) is verified: the anticorrelation displays a power law decay $1/\tau^2$ (see inset in Fig. 4) and the exponent $\beta/(\nu z) \simeq 0.50$ at small scale is recovered. It is remarkable that the power law behavior $y^{-\beta/\nu z}$ holds for the nonconnected function $\mathcal{G}(y) + 1$ until the time when anticorrelation appears. A similar behavior with a crossover from a power law decay to anticorrelation is observed in the experiment. However, curves corresponding to different crack speeds are collapsed using v_d instead of $t^* = v_d^{\beta/(\nu z)}$. This is also explained by the relation $\mu \sim v_d$ specific to our material. This is the first time that anticorrelation is predicted and observed in depinning systems at finite drive (see also Appendix C [24]). At short time the scaling behavior $G_v(\tau) \sim \tau^{-\beta/\nu z}$ holds when ξ_v is large compared to the microscopic scale of the disorder. Otherwise, a crossover to a different regime, not studied here, should occur at very small scales. The power law decay observed here is consistent with the depinning prediction $\tau^{-\beta/\nu z}$ even if ξ_v is of the order of d_0.

Discussion.—Our findings open new perspectives for the experimental study of disordered elastic interfaces. As the correlations of the local velocity display universal features of the depinning even when the driving speed is finite, the critical behavior can be investigated far from the critical point. This provides a robust and efficient method to identify the universality class of the transition and to test the relevance of specific depinning models.

The analysis of the local speed correlations has already been performed in previous simulations and experiments. But the link with the critical exponents was missing. In the simulations of Ref. [42] of an interface with short-range elasticity, the correlation function $C_v(x)$ was used to extract the scale ξ_v and the exponential cutoff was observed but the small scale exponent β/ν was not predicted. In the fracture experiments of Tallakstad *et al.* [36], the correlation functions of the local velocity were found to scale as $C_v(x) \sim x^{-\tau_x}$ and $G_v(\tau) \sim \tau^{-\tau_t}$ with exponents $\tau_x = 0.53 \pm 0.12$ and $\tau_t = 0.43$ a bit away from the depinning predictions $\beta/\nu \simeq 0.38$ and $\beta/(\nu z) \simeq 0.50$. However, exponential cutoffs at large distances and time were used for the fit and the anticorrelation in time was not observed. Note that standard log-log plot routines discard negative values and one must use alternative plots to see the anticorrelation. It would be interesting to test how far the behavior predicted in this study could capture the Tallakstad *et al.*'s experiments, as their systems allow the exploration of the crack behavior closer to the critical point than the one used in this study. Finally, we note that Gjerden *et al.* [43] computed the same correlation functions in simulations of a fiber bundle model that mimics the presence of damages in front of the crack. Their model should fall into the depinning universality class with long-range elasticity [43]

and they measured $\tau_x = \tau_t = 0.43$ with cutoffs faster than exponential.

Finally, it is important to remark that the scaling forms (2) and (3) are very general and valid for all out-of-equilibrium transitions with avalanche dynamics. The asymptotic forms (6) and (7) are also very general, as beyond ξ_v the spatial correlations decay as $1/x^{d+\alpha}$ for a long-range model (d being the spatial dimension) and exponentially fast for short-range elasticity. It would certainly be insightful to probe this behavior in various problems, including those where the nature of the elastic interactions still needs to be deciphered or in the context of the yielding transition where avalanches of plastic events are observed [4].

We thank E. Bouchaud and V. Démery for useful discussions. We acknowledge support from PSL Grant No. ANR-10-IDEX-0001-02-PSL. P. L. D. also acknowledges support from ANR Grant No. ANR-17-CE30-0027-01 RaMa-TraF.

*To whom all correspondence should be addressed.
clement.lpr@gmail.com

[1] D. S. Fisher, K. Dahmen, S. Ramanathan, and Y. Ben-Zion, Phys. Rev. Lett. **78**, 4885 (1997).
[2] D. S. Fisher, Phys. Rep. **301**, 113 (1998).
[3] E. A. Jagla, F. P. Landes, and A. Rosso, Phys. Rev. Lett. **112**, 174301 (2014).
[4] J. Lin, E. Lerner, A. Rosso, and M. Wyart, Proc. Natl. Acad. Sci. U.S.A. **111**, 14382 (2014).
[5] A. Nicolas, E. E. Ferrero, K. Martens, and J.-L. Barrat, Rev. Mod. Phys. **90**, 045006 (2018).
[6] S. Zapperi, P. Cizeau, G. Durin, and H. E. Stanley, Phys. Rev. B **58**, 6353 (1998).
[7] L. Laurson, X. Illa, S. Santucci, K. T. Tallakstad, K. J. Måløy, and M. J. Alava, Nat. Commun. **4**, 2927 (2013).
[8] G. Durin, F. Bohn, M. A. Correa, R. L. Sommer, P. Le Doussal, and K. J. Wiese, Phys. Rev. Lett. **117**, 087201 (2016).
[9] S. Janićević, L. Laurson, K. J. Måløy, S. Santucci, and M. J. Alava, Phys. Rev. Lett. **117**, 230601 (2016).
[10] J. Barés, L. Barbier, and D. Bonamy, Phys. Rev. Lett. **111**, 054301 (2013).
[11] J. Barés and D. Bonamy, Phil. Trans. R. Soc. A **377**, 20170386 (2019).
[12] J. Barés, D. Bonamy, and A. Rosso, Phys. Rev. E **100**, 023001 (2019).
[13] K. J. Måløy, S. Santucci, J. Schmittbuhl, and R. Toussaint, Phys. Rev. Lett. **96**, 045501 (2006).
[14] A. Tanguy, M. Gounelle, and S. Roux, Phys. Rev. E **58**, 1577 (1998).
[15] D. Bonamy, S. Santucci, and L. Ponson, Phys. Rev. Lett. **101**, 045501 (2008).
[16] D. Bonamy and E. Bouchaud, Phys. Rep. **498**, 1 (2011).
[17] L. Ponson, Int. J. Fract. **201**, 11 (2016).
[18] S. Roux, D. Vandembroucq, and F. Hild, Eur. J. Mech. A **22**, 743 (2003).
[19] S. Moulinet, A. Rosso, W. Krauth, and E. Rolley, Phys. Rev. E **69**, 035103(R) (2004).
[20] P. Le Doussal, K. Wiese, S. Moulinet, and E. Rolley, Europhys. Lett. **87**, 56001 (2009).
[21] J. R. Rice, J. Appl. Mech. **52**, 571 (1985).
[22] J. F. Joanny and P. G. de Gennes, J. Chem. Phys. **81**, 552 (1984).
[23] L. Laurson, S. Santucci, and S. Zapperi, Phys. Rev. E **81**, 046116 (2010).
[24] See Supplemental Material at http://link.aps.org/supplemental/10.1103/PhysRevLett.124.065501 which contains Appendix A for derivation of equation (1), Appendix B for derivation of equations (5) and (6) and in Appendix C we provide more evidence about the anticorrelation in the experiment.
[25] A. A. Griffith, Trans. R. Soc. Ser. A **221**, 163 (1921).
[26] L. B. Freund, *Dynamic Fracture Mechanics* (Cambridge University Press, Cambridge, England, 1990).
[27] V. Démery, A. Rosso, and L. Ponson, Europhys. Lett. **105**, 34003 (2014).
[28] A. Basu and B. K. Chakrabarti, Phil. Trans. R. Soc. A **377**, 20170387 (2019).
[29] H. Gao and J. R. Rice, J. Appl. Mech. **56**, 828 (1989).
[30] O. Narayan and D. S. Fisher, Phys. Rev. B **48**, 7030 (1993).
[31] H. Leschhorn, T. Nattermann, S. Stepanow, and L.-H. Tang, Ann. Phys. (N.Y.) **509**, 1 (1997).
[32] The dynamical exponent obeys the relation $z = \zeta + \beta/\nu$.
[33] Indeed as $\langle v(x,t)|v(0,t) \sim v_{\max}\rangle = v_d \mathcal{H}(x/\xi_v)$ in order to have a finite result when $v_d \to 0$ one must have $\mathcal{H}(z) \sim z^{-\beta/\nu}$ when $z \to 0$.
[34] P. Le Doussal and T. Thiery, https://arxiv.org/abs/1904.12136.
[35] J. Chopin, A. Bhaskar, A. Jog, and L. Ponson, Phys. Rev. Lett. **121**, 235501 (2018).
[36] K. T. Tallakstad, R. Toussaint, S. Santucci, J. Schmittbuhl, and K. J. Måløy, Phys. Rev. E **83**, 046108 (2011).
[37] A. Rosso and W. Krauth, Phys. Rev. E **65**, 025101(R) (2002).
[38] O. Duemmer and W. Krauth, J. Stat. Mech. (2007) P01019.
[39] P. Le Doussal, K. J. Wiese, and P. Chauve, Phys. Rev. B **66**, 174201 (2002).
[40] I. Kolvin, G. Cohen, and J. Fineberg, Phys. Rev. Lett. **114**, 175501 (2015).
[41] P. Chauve, T. Giamarchi, and P. Le Doussal, Phys. Rev. B **62**, 6241 (2000).
[42] O. Duemmer and W. Krauth, Phys. Rev. E **71**, 061601 (2005).
[43] K. S. Gjerden, A. Stormo, and A. Hansen, Front. Phys. **2**, 66 (2014).